ChemComm

COMMUNICATION

View Article Online
View Journal | View Issue

Cite this: *Chem. Commun.*, 2017, 53, 3193

Received 1st November 2016,
Accepted 11th February 2017

DOI: 10.1039/c6cc08761b

rsc.li/chemcomm

Mechanistic insights into intramolecular *ortho*-amination/hydroxylation by nonheme Fe^{IV}=NTs/Fe^{IV}=O species: the σ *vs.* the π channels†

Bhawana Pandey,[a] Madhavan Jaccob[ab] and Gopalan Rajaraman*[a]

Comparative oxidative abilities of nonheme Fe^{IV}=NTs and Fe^{IV}=O species using DFT has been explored. Our calculations reveal that the Fe^{IV}=NTs is found to be a stronger oxidant in two electron transfer reactions and react exclusively *via* π channels while the Fe^{IV}=O species is found to be a stronger oxidant when the σ-pathway is activated such as in HAT reactions.

High-valent iron–oxo species are found to be active intermediates in several heme and non-heme enzymes.[1] These discoveries motivated many synthetic chemists to prepare low molecular weight model complexes in order to understand their mechanistic features as well as gaining fundamental and practical significance of the oxygenation reactions.[2,3] Concurrently, theoretical methods have been widely used to correlate the geometrical and bonding aspects of enzymatic and biomimetic model complexes of heme and nonheme enzymes.[4]

Recently mononuclear non-heme iron enzymes and their respective model complexes have been proposed to catalyze carbon–heteroatom bond forming reactions (C–O and C–N bond formation) in an efficient manner.[5] The Fe^{IV}=NTs complexes are considered to be the congener of the popular the Fe^{IV}=O species and their generation and reactivity studies have recently gained momentum.[4f,6] Only a few examples of imidoiron(IV) complexes have been reported in the literature and for selected examples, catalytic abilities have been tested.[6a,7] These iron–imido complexes also undergo nitrene transfer reactions very efficiently.[8] As the imido species (NR^{-}) are isoelectronic with the oxo species (O^{2-}), they are capable of aminating aromatic compounds *via* C–H bond activation and their catalytic efficiency is found to be superior to those of high-valent iron oxo complexes.[6a,9]

Synthesis, spectroscopic and theoretical studies of a $[Fe^{IV}(NTs)(N_4Py)]^{2+}$ species were reported by Que and co-workers, where the superior oxidizing abilities of the imidoiron(IV) species were compared to those of the oxo analogue.[9a] This was also reiterated for sulfoxidation reactions in a recent study; however a contrasting behaviour was noted for hydrogen atom abstraction (HAT) reactions.[4e,7d] This contrasting reactivity pattern where the Fe^{IV}=NTs species is superior to the Fe^{IV}=O species only for some selected reactions prompted us to look into the comparative oxidative abilities of these two species on an analogous reaction. The reaction of a $[Fe^{II}(6\text{-Ph-TPA})]^{2+}$ (tpa = tris(2-pyridylmethyl)-amine) complex with a PhINTs species was found to cause intramolecular aromatic amination, while the reaction with PhIO led to intramolecular aromatic hydroxylation.[6a] The amination reaction was found to be catalysed by the $[(6\text{-Ph-TPA})Fe^{IV}$=NTs$]^{2+}$ species (**1**) while the analogous $[(6\text{-Ph-TPA})Fe^{IV}$=O$]^{2+}$ species (**2**) catalyse the hydroxylation reaction. Experimental observation suggests that the Fe^{IV}=NTs species is superior to the Fe^{IV}=O species for this reaction.[6a] Elucidating the exact mechanism of intramolecular *ortho*-amination and *ortho*-hydroxylation is relevant to improving the efficiency of the catalyst and also serves the purpose of establishing the comparative oxidative abilities of these two species. Here, we aim to address this issue using detailed density functional calculations (see the ESI† for computational details) and aim to answer the following questions: (i) what are the basic electronic structure differences between **1** and **2** that are attributed to the reactivity?; (ii) what are the mechanistic pathways for *ortho*-amination/hydroxylation by the Fe^{IV}=NTs/Fe^{IV}=O species? (iii) Why species **1** is an aggressive oxidant compared to species **2** in this chemistry while the inverse is true for HAT reactions?

While the Fe^{IV}=O species has accessible quintet and triplet states for reactivity, the Fe^{IV}=NTs species possesses a complex set of spin configurations considering singlet, triplet and quintet states for the Fe^{IV} unit and a singlet and a triplet state for the nitrene electrons. Our earlier theoretical calculations[6c] suggest

[a] *Department of Chemistry, Indian Institute of Technology Bombay, Powai, Mumbai, Maharashtra, 400076, India. E-mail: rajaraman@chem.iitb.ac.in; Tel: +91-22-2576-7187*

[b] *Department of Chemistry, Loyola College, Chennai 600 034, Tamil Nadu, India*

† Electronic supplementary information (ESI) available: Computational details, energy profile diagrams for different mechanisms, tables summarizing the structural parameters and spin densities, detailed mechanistic scheme for possible pathways, optimized structures and spin density plots of various species studied in this work, Eigen-value plots for selected species, energies and structure for the intramolecular amination/hydroxylation reaction studied. See DOI: 10.1039/c6cc08761b

that the triplet spin state [^{3}**1**$_{(IS,S)}$] (here the superscript represents spin multiplicity and the subscript denotes the spin state of the Fe^{IV} and NTs species, see computational details given in the ESI†) is found to be the ground state for the [(N$_4$Py)Fe^{IV}=NTs]$^{2+}$ species with another possible triplet spin state [^{3}**1**$_{(LS,T)}$] degenerate in energy. Similarly two different quintet electronic states [^{5}**1**$_{(IS,T)}$] and [^{5}**1**$_{(HS,S)}$] were also found to be degenerate. Therefore, here we have restricted our calculations to the ^{7}**1**$_{(HS,T)}$, ^{5}**1**$_{(HS,S)}$, ^{3}**1**$_{(IS,S)}$ and ^{1}**1**$_{(LS,S)}$ (S = 3, 2, 1 and 0) states for species **1**, while calculations were performed for triplet and quintet states for species **2**.[10]

Our calculations suggest that the triplet state [^{3}**1**$_{(IS,S)}$] is found to be the ground state for species **1** and this is in accord with the Mössbauer data reported for structurally similar Fe^{IV}=NTs reported earlier.[6c] All the reported energies are free energies computed at the B3LYP/TZVP level employing acetonitrile as solvent. Additional calculations performed utilizing dispersion corrections yield similar energies and are given in the ESI† (see Fig. S28). With respect to the triplet spin state [^{3}**1**$_{(IS,S)}$], the quintet [^{5}**1**$_{(HS,S)}$], septet [^{7}**1**$_{(HS,T)}$] and singlet [^{1}**1**$_{(LS,S)}$] spin states are 5.2, 11.7 and 40.1 kJ mol^{-1} higher in energy, respectively. Very similar energetics and patterns are obtained when explicit solvent phase optimization was carried out (see the ESI,† Tables S11 and S12). Within 11.7 kJ mol^{-1} of the energy window, three spin states are present and this can, in fact, help enhance the reactivity *via* a multi-state reactivity pattern. Optimized structures and spin density plots for [^{3}**1**$_{(IS,S)}$] (^{3}R) and [^{5}**1**$_{(HS,S)}$] (^{5}R) are given in Fig. S1 in the ESI.†

Both the triplet and quintet Fe–N/O bond lengths are drastically different for species **1** and **2** (1.767 Å *vs.* 1.629 Å and 1.750 Å *vs.* 1.623 for triplet and quintet states respectively; see Fig. S1 and S2 of the ESI†). Although both species (Fe^{IV}=NTs and Fe^{IV}=O) have the $(d_{xy})^2(\pi_{d_{xz}-p_x}^*)^1(\pi_{d_{yz}-p_y}^*)^1(d_{x^2-y^2})^0(d_{z^2}^*)^0$ ground state electronic configuration, the energy gaps are different, particularly the axial e$_g$ type orbitals are strongly antibonding in the Fe^{IV}=O species. The presence of a tosylate group in species **1** weakens the Fe–N bond and the Fe–N bond lengths are rather comparable to those of the Fe^{IV}=O···Sc^{3+} species.[11] The computed spin densities for species 1 reveals that two unpaired electrons are strongly delocalized on the nitrene nitrogen and iron centres as well as to the oxygen atoms of the tosylate group (see ESI† for other difference in bonding features).

To understand the reactivity differences, we have explored the mechanism of intramolecular *ortho*-amination/hydroxylation by the Fe^{IV}=NTs and the Fe^{IV}=O species (Scheme 1 or for detailed mechanism Scheme S1 in the ESI†). The first step in the *ortho*-amination process is the direct aromatic electrophilic attack (*via ts1*; path 1) of the ferryl imido/oxo nitrogen/oxygen atom leading to the formation of a C–N/O bond between the nitrogen/oxygen atom of ferryl imido/oxo and the aromatic carbon atom. This transition state proceeds by two different intermediates, first is a radical intermediate (*int1a*; path 1a) assumed to form *via* a one-electron transfer process while the second is a cationic intermediate (*int1b*; path 1b) which forms when a two-electron transfer takes place. In the next step, from either the *int1a* or *int1b*, dearomatization takes place through 1,2-hydrogen atom

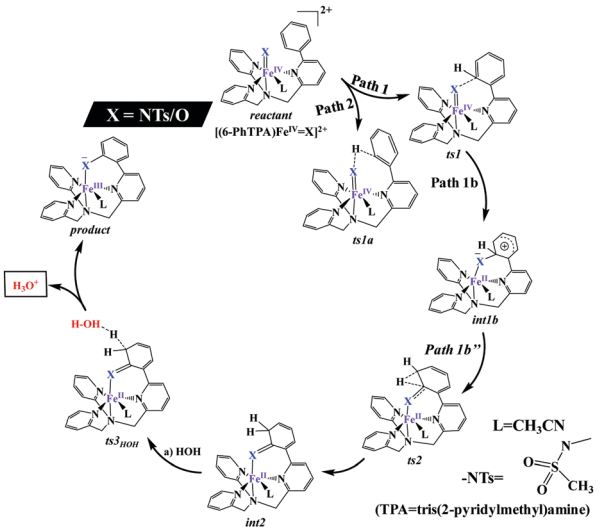

Scheme 1 Mechanism adapted for the intramolecular amination/hydroxylation reaction by [(6-PhTPA)Fe^{IV}=NTs/O]$^{2+}$ species.

transfer *via ts2* (path 1b″) leading to the formation of a dearomatized intermediate (*int2*). Alternatively, instead of 1,2-hydrogen atom transfer, H atom migration to the nitride or oxo atom can take place (*via ts2a*; path1b′) leading to the formation of an intermediate followed by further migration of H to the adjacent carbon(2) atom (*via ts2b*) leading back to *int2*. In the next step, hydrogen atom abstraction by PhINTs or water takes place *via ts3* (*ts3*$_{HOH}$) leading to the formation of a Fe^{III}-amido/Fe^{III}–oxo product.

The barrier height for the direct electrophilic attack (path 1) of the ferrylimido nitrogen on the aromatic ring (*ts1*) is estimated to be 25.9, 42.4, 73.4 and 88.7 kJ mol^{-1} on the quintet (^{5}**1**$_{(HS,S)}$), septet (^{7}**1**$_{(HS,T)}$), triplet [^{3}**1**$_{(IS,S)}$], and singlet [^{1}**1**$_{(LS,S)}$] surfaces respectively (Fig. 1). The barrier height for the direct electrophilic attack of the Fe^{IV}=O species on the aromatic ring (*2-ts1*) is estimated to be 54.6 and 84.3 kJ mol^{-1} on the quintet and triplet surfaces, respectively. Alternatively, C–H bond activation (path 2) by nitrene can also take place (*via* 1-*ts1a* as shown in Scheme 1) and for this transition state, the lowest barrier height is estimated to be 92.7 kJ mol^{-1} at

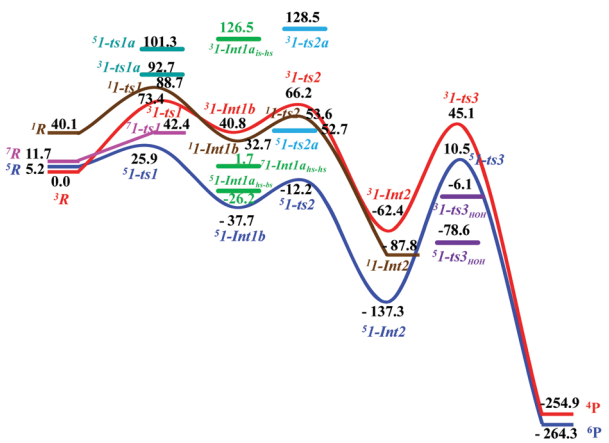

Fig. 1 B3LYP computed free energy profile (ΔG in kJ mol^{-1}) of intramolecular amination by [(6-PhTPA)Fe^{IV}=NTs]$^{2+}$.

the triplet surface which is nearly four times larger compared to that for the electrophilic attack pathway described above and suggests that this pathway is unlikely. This is further supported by experiments where the reported k_H/k_D values are large for both species **1** (k_H/k_D = 0.9) and **2** (k_H/k_D = 1.3) suggesting an electrophilic pathway.[6a] These computed barriers also correlate well with the fact that species **1** is more electrophilic than species **2**.[7d]

Although the triplet state is the ground state for both species **1** and **2**, the quintet state is found to possess the lowest barrier height for both the species and this is in accord with the reactivity pattern observed earlier for the Fe^{IV}═O species.[12] This demands a minimum energy crossing point (MECP) between triplet and quintet surfaces and these are generally favourable as the spin–orbit coupling associated with these species are often large.[13] The Fe–NTs/O bond is elongated to 1.90 Å/1.685 Å at the quintet transition state, while the newly formed N/O–C distance is found to be 2.131 Å/2.224 Å at the same surface. Besides, the N_{ax}–Fe–NTs/N_{ax}–Fe–O angle also changes significantly from 176.5°/173.8° in the reactant to 166.7°/168.5° at the quintet transition state. The aromatic C(1) carbon also loses the double bond character as the C(1)–C(2) bond is elongated from 1.395 Å/1.359 Å to 1.428 Å/1.412 Å (see Tables S1 and S3 of the ESI†).

There is significant reduction in the spin density on the nitrene nitrogen atom and a concurrent increase in the spin density at the Fe centre. Analysis of the Molecular Orbitals of the transition state clearly reveals a two-electron transfer from the substrate to the Fe–N/O moiety. This indicates that the reaction proceeds *via* the cationic intermediate (*int1b*; path 1b) rather than the radical intermediate (*int1a*; path 1a). In the next step, the N–C and O–C bonds form completely leading to longer Fe–NTs (2.058 Å) and Fe–O (1.920) bonds. To cross check the stability of *int1a*, we have computed the energies of the ^{7}*int1a*, ^{5}*int1a* and ^{3}*int1a* states and these states are found to lie much higher in energy compared to the corresponding cationic intermediates (see Fig. 1). This affirms the formation of a cationic intermediate in this reaction. The cationic intermediate has a quintet (^{5}*int1b*) ground state and its formation is exothermic in nature by 37.7 kJ mol^{-1}. In the next step, hydrogen atom migration is considered from *int1b*. In the *ortho*-amination reaction, among the transition states computed for this step, the quintet ^{5}*1-ts2* has the lowest barrier (25.5 kJ mol^{-1}) from the ^{5}*1-int1b* species (see Fig. 1). In the *ortho*-hydroxylation reaction, the quintet ^{5}*2-ts2* has the lowest barrier (1.6 kJ mol^{-1}) from the ^{5}*2-int1b* species (see Fig. 2). As the H-atom migration takes place, the N/O–C(1) bond is strengthened (from 1.465 Å/1.336 Å at ^{5}*int1b* to 1.399 Å/1.318 Å at ^{5}*ts2*) and this forces the Fe–N bond to become further long at *ts2* (from 2.058 Å to 2.103 Å). In the newly formed H–C(2) bond, the NTs(O)–C–H bond angle is increased from 103.6° (111.5° for species **2**) to 108.7° (112.2°) and this clearly reveals that the H-atom shuttles between the two carbon atoms of the aromatic ring. ^{5}*1-Int2* is stabilized by a 137.3 kJ mol^{-1} energy margin for *ortho*-amination (161.4 kJ mol^{-1} energy for the hydroxylation reactions, see also Fig. 2). Formation of the ^{5}*Int2b* intermediate is also supported by the observation of the NIH shift reported for both amination and hydroxylation reactions.[6a] We have also explored an alternative pathway for the H-atom migration (path 1b′) *via ts2a* and *ts2b* (see Scheme 1) but the barrier heights for this pathway are found to be significantly larger (for *ts2a* the lowest barrier height is 90.4 kJ mol^{-1} at the quintet surface and *ts2b* has a barrier height of 82.5 kJ mol^{-1} at the quintet surface) and can be neglected. The computed energetics clearly reveals that after the first transition state, the entire amination/hydroxylation reaction occurs on the quintet surface with concomitant formation of a cationic intermediate. This is contrary to epoxidation of olefins by the Fe^{IV}═O species where radical intermediates are detected.[10a,14]

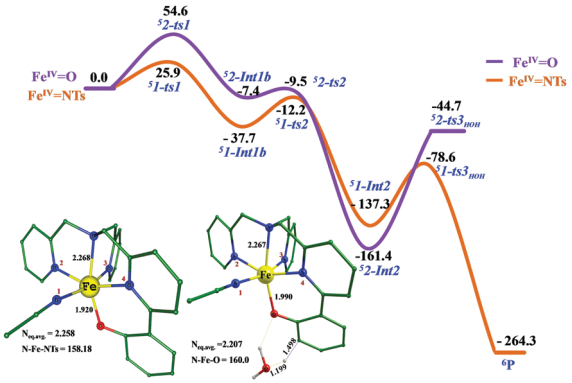

Fig. 2 B3LYP computed free energy profile (Δ*G* in kJ mol^{-1}) of intramolecular amination and hydroxylation by [(6-PhTPA)Fe^{IV}═NTs]$^{2+}$ and [(6-PhTPA)Fe^{IV}═O]$^{2+}$.

In the final step, proton abstraction by the PhINTs species *via ts3* is expected leading to the formation of the aminated product ([[(6-(N–TsN–C_6H_4)–TPA)Fe^{III}($NCCH_3$)]$^{2+}$) with retention of the aromaticity of the benzene ring. In ^{5}*ts3*, the C–H bond is elongated from 1.093 Å to 1.245 Å and the H–N bond distance is found to be 1.483 Å. This step has a barrier height of 147.8 kJ mol^{-1} from the ^{5}*1-int2* species reflecting activation of the inert C–H bond (sp^3-hybridized). As this barrier height is very large, we have additionally explored the possibility of H-atom abstraction by a water molecule *via ts3*$_{HOH}$. This transition state is found to have a low barrier height (58.7 kJ mol^{-1} for *ortho*-amination and 116.7 kJ mol^{-1} for *ortho*-hydroxylation at the quintet surface, see Fig. 2). This suggests that the proton abstraction is likely to be carried out by a water molecule rather than by the PhINTs species. The final product formation is found to be exothermic by 264.3 kJ mol^{-1} and this large stabilization energy is due to gain of aromaticity and this energetic gain may ease the energy penalty required for the subsequent catalytic cycles.

The PES developed for the *ortho*-hydroxylation reaction by the Fe^{IV}═O species in comparison to the amination reaction is shown in Fig. 2 (taking only the lowest energy points). For both the species, the first step is the rate determining step with 25.9 kJ mol^{-1} for **1** and 54.6 kJ mol^{-1} for **2**. The barrier computed for Fe^{IV}═O is *ca.* two times larger than that of the amination reaction by the Fe^{IV}═NTs species.

This is in accord with the experimental observations and also the reactivity trend reported for the sulphimidation reaction. To have a clearer picture, we have additionally performed calculations for hydrogen atom transfer (HAT) reactions using

dehydroanthracene (DHA) as the substrate. On the quintet surface, the Fe^{IV}═O species yields a barrier height of 58.3 kJ mol^{-1} while the Fe^{IV}═NTs species yields a barrier of 94.5 kJ mol^{-1}. Here, the Fe^{IV}═O species is a nearly two times stronger oxidant than the Fe^{IV}═NTs species.

To understand this puzzling reactivity, we have analysed the transition states of the *ortho*-amination/hydroxylation and HAT reactions. On the quintet spin surface, the substrate usually aligns in a linear fashion along the Fe–O/N bond. For the *ortho*-amination/hydroxylation reaction transition state, the Fe–N(Ts)–C and Fe–O–C angles are found to be 105.15° and 117.05°, respectively. This reveals a π-type pathway being operational for both Fe^{IV}═NTs and Fe^{IV}═O species.[4e,7d] Since both the reactions are intramolecular reactions, achieving linearity which is required to activate the σ-pathway is not possible with this ligand. This significantly diminishes the reactivity of the Fe^{IV}═O species and this has been witnessed earlier.[5] These constraints are eliminated in the HAT transfer reactions with Fe^{IV}═O species where the Fe–O–H angle is found to be 168.8° revealing a σ-type pathway leading to a very small barrier height. For the Fe^{IV}═NTs species, the Fe–N–H angle is found to be still small (117.3°) and suggests non-existence of the σ-pathway for the Fe^{IV}═NTs species. This is primarily due to the tosylate moiety attached to the N-atom, which not only sterically blocks the position but also weakens the Fe–N σ interaction as discussed earlier.

Moreover, analysing the transition state reveals further differences in reactivity between these two species. For the *ortho*-amination/hydroxylation reaction, analysis reveals that two electrons are transferred already into the Fe–N moiety for the Fe^{IV}═NTs species while only one-electron transfer was witnessed for the Fe^{IV}═O species. This suggests that Fe^{IV}═NTs reacts exclusively *via* the π-pathway and reacts faster than Fe^{IV}═O when a two-electron transfer is involved. (Note that two-electron transfer sulphimidation by Fe^{IV}═NTs is faster than sulphoxidation by the Fe^{IV}═O species.) Unlike the Fe^{IV}═O species, the Fe^{IV}═NTs species possesses additional electronic flexibility where the nitrene at the quintet ground state of Fe^{IV}═NTs has a significant spin density and partial triplet character. These MOs of the nitrenes are nearly degenerate and prefer a two-electron transfer process where one electron is transferred to σ-d_{z^2} of Fe and another to the ($\pi_{d_{xz}-p_x}^*$) orbital of nitrene. This is reflected clearly in the computed spin densities (see the ESI† for details). For HAT reactions on the other hand, for the Fe^{IV}═O species σ(d_{z^2}) is directly involved facilitating easier electron transfer while in the Fe^{IV}═NTs species, the π pathway is preferred leading to less overlap with σ(d_{z^2}) and hence a larger barrier height.

In summary, our study reveals that the Fe^{IV}═O species exhibit both π- and σ-pathways depending on the nature of the substrate while the Fe^{IV}═NTs species found to react exclusively *via* π channels. The reactivity however can be fined tuned by ligand design (such as additional spacer groups for the aromatic groups) and efforts to model such reactions are currently underway in our laboratory.

GR and MJ acknowledges DST (EMR/2014/000247;DST/SERB/FT/CS-165/2013) and generous computational resources from IIT Bombay. BP thanks UGC for an SRF fellowship.

References

1 (*a*) L. Que Jr. and R. Y. N. Ho, *Chem. Rev.*, 1996, **96**, 2607–2624; (*b*) B. Meunier, S. P. de Visser and S. Shaik, *Chem. Rev.*, 2004, **104**, 3947–3980; (*c*) J. Hohenberger, K. Ray and K. Meyer, *Nat. Commun.*, 2012, **3**, 720; (*d*) N. Y. Oh, Y. Suh, M. J. Park, M. S. Seo, J. Kim and W. Nam, *Angew. Chem.*, 2005, **117**, 4307–4311.
2 (*a*) M. Costas, M. P. Mehn, M. P. Jensen and L. Que, *Chem. Rev.*, 2004, **104**, 939; (*b*) W. Nam, *Acc. Chem. Res.*, 2007, **40**, 522–531; (*c*) S. Jana, M. Ghosh, M. Ambule and S. S. Gupta, *Org. Lett.*, 2017, DOI: 10.1021/acs.orglett.6b03359.
3 S. P. de Visser, R. Latifi, L. Tahsini and W. Nam, *Chem. – Asian J.*, 2011, **6**, 493–504.
4 (*a*) J.-U. Rohde, J.-H. In, M. H. Lim, W. W. Brennessel, M. R. Bukowski, A. Stubna, E. Muenck, W. Nam and L. Que, Jr., *Science*, 2003, **299**, 1037–1039; (*b*) A. Decker, J.-U. Rohde, E. J. Klinker, S. D. Wong, L. Que, Jr. and E. I. Solomon, *J. Am. Chem. Soc.*, 2007, **129**, 15983–15996; (*c*) A. Decker, J.-U. Rohde, L. Que, Jr. and E. I. Solomon, *J. Am. Chem. Soc.*, 2004, **126**, 5378–5379; (*d*) A. Bassan, M. R. A. Blomberg, T. Borowski and P. E. M. Siegbahn, *J. Inorg. Biochem.*, 2006, **100**, 727–743; (*e*) S. Kumar, A. S. Faponle, P. Barman, A. K. Vardhaman, C. V. Sastri, D. Kumar and S. P. de Visser, *J. Am. Chem. Soc.*, 2014, **136**, 17102–17115; (*f*) B. Mondal, L. Roy, F. Neese and S. Ye, *Isr. J. Chem.*, 2016, **56**, 763–772; (*g*) P. Comba, S. Fukuzumi, C. Koke, B. Martin, A.-M. Löhr and J. Straub, *Angew. Chem., Int. Ed.*, 2016, **55**, 11129–11133.
5 A. Ansari, A. Kaushik and G. Rajaraman, *J. Am. Chem. Soc.*, 2011, **135**, 4235–4249.
6 (*a*) M. P. Jensen, M. P. Mehn and L. Que, Jr., *Angew. Chem., Int. Ed.*, 2003, **42**, 4357–4360; (*b*) S.-L. Abram, I. Monte-Perez, F. F. Pfaff, E. R. Farquhar and K. Ray, *Chem. Commun.*, 2014, **50**, 9852–9854; (*c*) M. Jaccob and G. Rajaraman, *Dalton Trans.*, 2012, **41**, 10430–10439; (*d*) D. M. Spasyuk, S. H. Carpenter, C. E. Kefalidis, W. E. Piers, M. L. Neidig and L. Maron, *Chem. Sci.*, 2016, **7**, 5939–5944; (*e*) H. Bataineh, O. Pestovsky and A. Bakac, *Inorg. Chem.*, 2016, **55**, 6719–6724.
7 (*a*) C. Geng, S. Ye and F. Neese, *Dalton Trans.*, 2014, **43**, 6079–6086; (*b*) R. E. Cowley, N. A. Eckert, S. Vaddadi, T. M. Figg, T. R. Cundari and P. L. Holland, *J. Am. Chem. Soc.*, 2011, **133**, 9796–9811; (*c*) I. Monte-Pérez, S. Kundu and K. Ray, *Z. Anorg. Allg. Chem.*, 2015, **641**, 78–82; (*d*) A. K. Vardhaman, P. Barman, S. Kumar, C. V. Sastri, D. Kumar and V. S. P. de, *Angew. Chem., Int. Ed.*, 2013, **52**, 12288–12292; (*e*) M. Goswami, V. Lyaskovskyy, S. R. Domingos, W. J. Buma, S. Woutersen, O. Troeppner, I. Ivanović-Burmazović, H. Lu, X. Cui, X. P. Zhang, E. J. Reijerse, S. DeBeer, M. M. van Schooneveld, F. F. Pfaff, K. Ray and B. de Bruin, *J. Am. Chem. Soc.*, 2015, **137**, 5468–5479.
8 (*a*) L. Zhang and L. Deng, *Chin. Sci. Bull.*, 2012, **57**, 2352–2360; (*b*) I. Saikia, B. Kashyap and P. Phukan, *Chem. Commun.*, 2011, **47**, 2967–2969.
9 (*a*) E. J. Klinker, T. A. Jackson, M. P. Jensen, A. Stubna, G. Juhasz, E. L. Bominaar, E. Muenck and L. Que, Jr., *Angew. Chem., Int. Ed.*, 2006, **45**, 7394–7397; (*b*) D. L. J. Broere, N. P. van Leest, B. de Bruin, M. A. Siegler and J. I. van der Vlugt, *Inorg. Chem.*, 2016, **55**, 8603–8611.
10 (*a*) P. Comba and G. Rajaraman, *Inorg. Chem.*, 2008, **47**, 78–93; (*b*) J. Bautz, P. Comba, C. L. Laorden, M. Menzel and G. Rajaraman, *Angew. Chem., Int. Ed.*, 2007, **46**, 8067–8070.
11 (*a*) Y. Morimoto, J. Park, T. Suenobu, Y.-M. Lee, W. Nam and S. Fukuzumi, *Inorg. Chem.*, 2012, **51**, 10025–10036; (*b*) F. Li, K. M. Van Heuvelen, K. K. Meier, E. Münck and L. Que, *J. Am. Chem. Soc.*, 2013, **135**, 10198–10201.
12 (*a*) H. Hirao, D. Kumar, L. Que, Jr. and S. Shaik, *J. Am. Chem. Soc.*, 2006, **128**, 8590–8606; (*b*) S. P. de Visser, K. Oh, A.-R. Han and W. Nam, *Inorg. Chem.*, 2007, **46**, 4632–4641; (*c*) S. Shaik, H. Hirao and D. Kumar, *Acc. Chem. Res.*, 2007, **40**, 532–542.
13 (*a*) J. N. Harvey, *Wiley Interdiscip. Rev.: Comput. Mol. Sci.*, 2014, **4**, 1–14; (*b*) T. Yang, M. G. Quesne, H. M. Neu, F. G. Cantú-Reinhard, D. P. Goldberg and S. P. de Visser, *J. Am. Chem. Soc.*, 2016, **138**, 12375–12386.
14 M. R. Bukowski, P. Comba, A. Lienke, C. Limberg, C. Lopez de Laorden, R. Mas-Ballesté, M. Merz and L. Que, *Angew. Chem., Int. Ed.*, 2006, **45**, 3446–3449.

